Counterion–Mediated Hierarchical Self-Assembly of an ABC Miktoarm Star Terpolymer

ARTICLE *in* ACS NANO · APRIL 2013

Impact Factor: 12.88 · DOI: 10.1021/nn400031u · Source: PubMed

Counterion-Mediated Hierarchical Self-Assembly of an ABC Miktoarm Star Terpolymer

Andreas Hanisch,[†] André H. Gröschel,[†] Melanie Förtsch,[†] Markus Drechsler,[†] Hiroshi Jinnai,[‡] Thomas M. Ruhland,[†] Felix H. Schacher,[§,*] and Axel H. E. Müller[†,⊥,*]

[†]Makromolekulare Chemie II, Universität Bayreuth, D-95440 Bayreuth, Germany, [‡]Japan Science and Technology Agency (JST), ERATO, Takahara Soft Interfaces Project and Institute for Materials Chemistry, International Institute for Carbon Neutral Energy Research (WPI-I2CNER) and Engineering (IMCE), Kyushu University, 744 Motooka, Nishi-ku, Fukuoka 819-0395, Japan, and [§]Institut für Organische Chemie und Makromolekulare Chemie (IOMC), and Jena Center for Soft Matter (JCSM), Friedrich-Schiller-Universität Jena, Humboldtstrasse 10, D-07743 Jena, Germany. [⊥]Present address: Institut für Organische Chemie, Johannes Gutenberg-Universität Mainz, D-55099 Mainz, Germany.

ABSTRACT

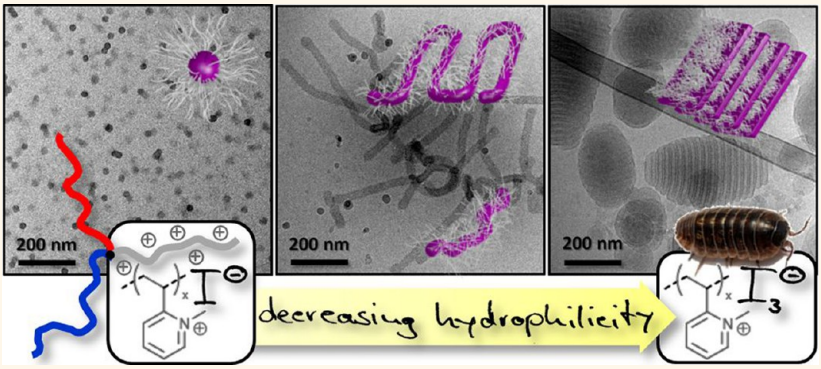

Directed self-assembly processes of polymeric systems represent a powerful approach for the generation of structural hierarchy in analogy to biological systems. Herein, we utilize triiodide as a strongly polarizable counterion to induce hierarchical self-assembly of an ABC miktoarm star terpolymer comprising a polybutadiene (PB), a poly(*tert*-butyl methacrylate) (P*t*BMA), and a poly(*N*-methyl-2-vinylpyridinium) (P2VPq) segment. Hereby, the miktoarm architecture in conjunction with an increasing ratio of triiodide *versus* iodide counterions allows for a stepwise assembly of spherical micelles as initial building blocks into cylindrical structures and superstructures thereof. Finally, micrometer-sized multicompartment particles with a periodic lamellar fine structure are observed, for which we introduce the term "woodlouse". The counterion-mediated decrease in hydrophilicity of the corona-forming P2VPq block is the underlying trigger to induce this hierarchical structure formation. All individual steps and the corresponding intermediates toward these well-defined superstructures were intensively studied by scattering and electron microscopic techniques, including transmission electron microtomography.

KEYWORDS: ABC miktoarm star terpolymer · hierarchical self-assembly · polyelectrolytes · multicompartment micelles · poly(2-vinylpyridine)

Self-assembly processes[1] are of particular importance in biological systems for the formation of defined, monodisperse structures on multiple length scales.[2] Inspired by nature, low molecular weight amphiphiles (*e.g.*, surfactants and lipids) represent a class of well-studied compounds.[3,4] However, amphiphilic AB diblock copolymers are superior to their low molecular weight analogues as they combine high functionality and compositional diversity as well as different assembly pathways to obtain a multitude of thermodynamically or kinetically controlled morphologies in solution.[5,6] Such structures are of high potential use for a variety of applications in the field of nano- and biotechnology.[7−11]

During the past decade, advances in polymer synthesis and macromolecular conjugation reactions led to progressively complex polymer architectures and compositions being accessible. The introduction of an additional

* Address correspondence to felix.schacher@uni-jena.de, axel.mueller@uni-mainz.de.

Received for review January 3, 2013 and accepted April 1, 2013.

Published online April 01, 2013
10.1021/nn400031u

block to obtain ABC triblock terpolymers results in the formation of nanostructures of increased complexity.[12,13] Three individual building blocks give rise to core–shell–corona structures as well as core- or corona-compartmentalized aggregates *via* adequate choice of a selective solvent. For example, different multicompartment micelles could be fabricated by direct dispersion of ABC miktoarm star terpolymers in a selective solvent for one of the blocks. Depending on the relative block ratios, "hamburger" micelles, segmented worm-like micelles, nanostructured vesicles, and raspberry-like micelles were observed for different systems.[14–17]

Examples of compartmentalized structures from linear triblock terpolymers involve, for example, materials containing fluorocarbon segments[18,19] or interpolyelectrolyte complexes.[20,21] Interestingly, also the formation of double and triple helices from achiral (meth)acrylate-type triblock terpolymers was reported.[22] In this case, Liu and co-workers showed that for distinct solvent mixtures a time-dependent hierarchical transition from spherical to cylindrical micelles and finally helices took place. Jiang *et al.* obtained giant segmented worm-like micelles from linear ABC triblock terpolymers with a poly(2-vinylpyridine) block by decreasing the solubility of the latter.[23] Recently, we presented a general concept for the generation of multicompartment micelles from linear ABC triblock terpolymers by a step-by-step reduction of the conformational degrees of freedom.[24] Using different ternary systems and compositions, reversible step-growth polymerization of multicompartment micelles as well as the solution-based preparation of Janus structures could be demonstrated.[25] Another strategy for creating hierarchical and compartmentalized structures is crystallization-driven self-assembly.[26–28] This facile process enables the construction of A-B, A-B-A, and, very recently, even A-B-C block comicelles *via* the stepwise addition of crystalline-coil polyferrocenylsilane block copolymers. Furthermore, cylindrical A-B-C block comicelles were shown to act as giant amphiphiles and assembled into micrometer-sized supermicelles, similar to micelle formation from linear ABC triblock terpolymers.[28] In all of these systems, the formation of hierarchical superstructures is directed by the terpolymer architecture,[14–17] the self-assembly pathway,[24,25] electrostatic interactions,[20,21] the solvent composition,[22,23,28] or certain characteristics of one of the segments, like perfluorinated[18,19] or crystallizable blocks.[26–29]

Apart from that, the use of additives represents an interesting alternative trigger. Wooley, Pochan, and co-workers exploited the interaction of triblock terpolymers consisting of polystyrene, poly(methyl acrylate), and poly(acrylic acid) (PAA) segments with divalent organic counterions. By adjusting the electrostatic complexation of the PAA block with diamines in mixtures of THF and water, spherical, cylindrical, and disk-like micelles as well as the corresponding superstructures or toroidal aggregates were generated.[30–34] The nature and the overall amount of the added diamine in combination with solvent quality or the block sequence were identified as main set screws.[35]

In this contribution, we present the hierarchical self-assembly of a polybutadiene-*arm*-poly(*N*-methyl-2-vinylpyridinium iodide)-*arm*-poly(*tert*-butyl methacrylate) miktoarm star terpolymer (μ-BVqT) in aqueous solution. We show that the hydrophilicity of the corona-forming poly(*N*-methyl-2-vinylpyridinium iodide) block (P2VPq) is controlled by the nature of the counterion, which is crucial in directing the self-assembly process. The addition of iodine results in the formation of triiodide counterions from iodide. By increasing the amount of triiodide in the system, the assembly of spherical micelles into cylindrical micelles, followed by intertwining of these cylinders into compact particles, resembles a step-by-step increase in hierarchy. All intermediate steps are visualized using (cryogenic) transmission electron microscopy (cryo-TEM and TEM). In this context, we found a unique micellar morphology, which we call "woodlouse" structure. This example of a compartmentalized block copolymer particle was comprehensively studied by (cryo-)TEM and TEM tomography (TEMT), enabling a detailed illustration of the underlying mechanism and the final superstructure morphology.

RESULTS AND DISCUSSION

Synthesis and Characterization of the PB-P2VP-P*t*BMA Miktoarm Star Terpolymer. The precursor polybutadiene-*arm*-poly(2-vinylpyridine)-*arm*-poly(*tert*-butyl methacrylate) miktoarm star terpolymer (μ-BVT) was synthesized *via* a combination of anionic polymerization, atom transfer radical polymerization (ATRP), and azide–alkyne Huisgen cycloaddition in a similar way as has been reported recently by our group (Scheme 1).[36] Details on the synthetic procedure and material characterization are given in the Supporting Information. The polymer μ-$B_{109}V_{81}T_{53}$ has a number-average molecular weight of M_n = 22.2 kg/mol and a polydispersity index of 1.07. The subscripts denote the degrees of polymerization of the corresponding blocks.

Besides optional post-polymerization functionalization of the polybutadiene block (PB), for example, *via* thiol–ene chemistry[37] or crosslinking,[38] μ-BVT features a pH-responsive poly(2-vinylpyridine) block (P2VP)[39] and a poly(*tert*-butyl methacrylate) segment (P*t*BMA) that can be hydrolyzed to poly(methacrylic acid), a weak polyelectrolyte.[40] For the research reported here, we transformed P2VP into the strong polyelectrolyte poly(*N*-methyl-2-vinylpyridinium iodide) (P2VPq) by quaternization with methyl iodide.[21]

Self-Assembly Behavior of μ-BVqT. Inspired by the diversity of structures formed by ABC miktoarm star terpolymers in solution,[14,15,17,41] we were interested

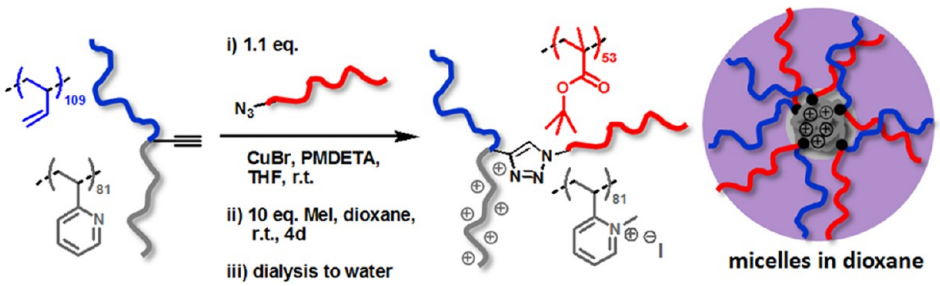

Scheme 1. Route for the synthesis of μ-BVqT and color code of the arms.

in the self-assembly of μ-BVT in aqueous media. First, the P2VP block was quaternized in dioxane using methyl iodide to yield μ-BVqT.[21] Owing to the low solubility of P2VPq in dioxane, micelles with an ionic P2VPq core and a corona consisting of PB and P*t*BMA are formed as shown by TEM (Figure 1A) and DLS (Supporting Information Figure S2). In TEM, only the micellar core ($d_{core} \sim 7.5$ nm, compared to $R_{h,app}$ = 12.5 nm from DLS) is visible due to the high electron density of the iodide counterions in P2VPq. We assume a mixed corona of PB and P*t*BMA as a consequence of the miktoarm star architecture (Scheme 1).

The as-prepared μ-BVqT micelles were subsequently transferred into water, leading to an inversion of the solubility of the constituting segments. P2VPq now forms the corona, whereas both PB and P*t*BMA are hydrophobic and build up the core. From simple solubility tests of the respective homopolymers, we know that during dialysis the PB block collapses first, followed by P*t*BMA. At the same time, P2VPq swells and stabilizes the whole aggregate. At about 20 vol % water in dioxane, P2VPq is fully solubilized while P*t*BMA and PB are insoluble. This is supported by the respective solubility parameters, δ, in $(MPa)^{1/2}$: $PB_{90\%1,2}$ = 17.4;[42] P*t*BMA = 18.0;[43] 1,4-dioxane = 20.5;[44] water = 47.9.[44] Consequently, during the dialysis to water, an intermediate stage will be reached where the solubility of the constituting blocks is inverted and micelles with a P2VPq corona are formed.

In terms of micellar morphology, two limiting cases were observed after dialysis to water under comparable preparation conditions: in one case, spherical micelles were found in TEM (Figure 1B, $d_{micelle}$ = 24.5 $\pm$ 2.0 nm). We propose that these consist of a mixed PB/P*t*BMA core and a P2VPq corona. In another batch, a completely different morphology was observed. TEM and cryo-TEM images revealed rather complex aggregates with an internal lamellar fine structure (Figure 1C,D and Figure S3). The particles feature an elongated barrel-like shape and were mostly in a size range of 200−500 nm. Due to their shape, we named those substructured particles "woodlouse" aggregates. In some cases, also spherical, multilamellar aggregates were observed (see inset in Figure 1C). We were initially puzzled by the fact that two entirely different morphologies evolved from the same μ-BVqT system. Partial crosslinking of the PB block was excluded by repeated SEC measurements of μ-BVT after some months of storage.

Two questions arise from these observations: (A) Which parameter is responsible for two different levels of structure formation, and (B) how are the individual μ-BVqT star terpolymer molecules arranged within such a highly periodic structure? We first dissect the underlying mechanism of superstructure formation and later present a more detailed structural investigation of the "woodlouse" aggregates.

Before studying the self-assembly mechanism in detail, we were interested in the influence of the polymer structure itself on the obtained aggregates. Therefore, materials of similar chemical composition but different architecture were used, more precisely a diblock copolymer ($B_{109}V_{81}$) and a linear triblock terpolymer ($B_{1108}V_{142}T_{93}$). However, only ill-defined aggregates were obtained from these linear polymers after quaternization and comparable preparation conditions (see representative micrographs of the triblock terpolymer in Figure S4). These findings demonstrate that the miktoarm architecture itself is an important criterion for the hierarchical self-assembly into substructured particles. Hadjichristidis and co-workers already showed both experimentally and by theoretical investigations that the micellization behavior of A_2B miktoarm systems is different compared to linear AB diblock copolymers due to topological differences at the core−corona interface.[45]

Hierarchical Superstructure Formation. According to cryo-TEM (Figure 1D), the "woodlouse" aggregates can be preliminarily described as superstructures from either cylindrical micelles or lamellae. However, as the periodicity of these particles is in the size range of the diameter observed for the spherical micelles in Figure 1B, we assume these to act as primary building blocks. The different structures observed would then simply correspond to different levels of superstructure formation. Regarding the overall morphology, similar structures, such as laterally structured vesicles or layered structures, were already predicted by simulations of ABC miktoarm star terpolymers with one solvophobic block.[46,47] More detailed information about the superstructure

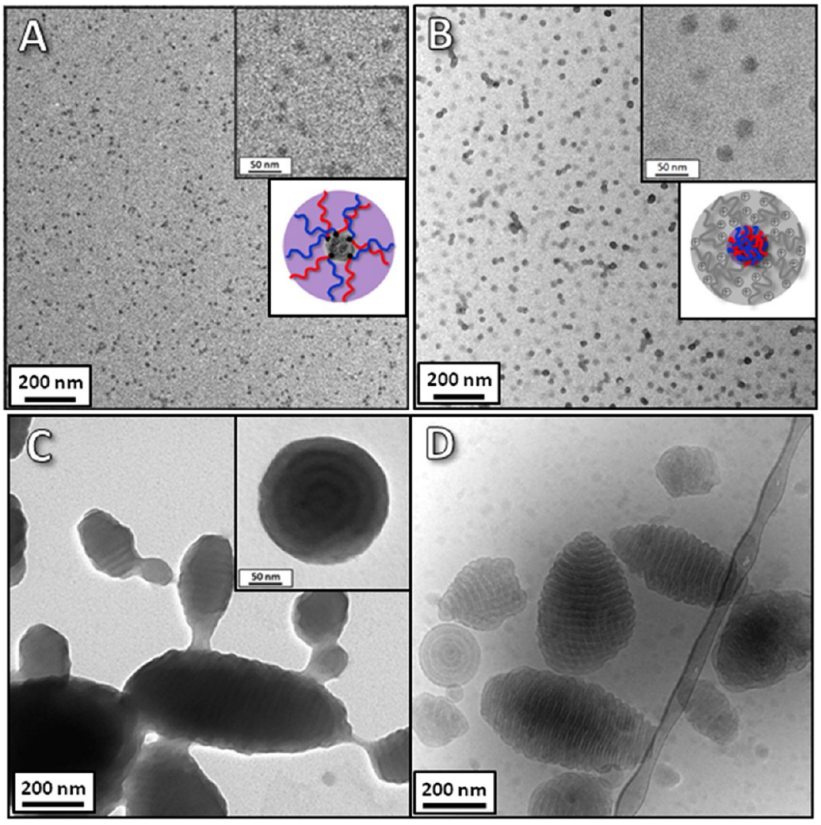

Figure 1. TEM micrographs of spherical micelles of μ-BVqT in dioxane (A) and the aggregates obtained thereof by dialysis to water: inverted spherical micelles (B) and "woodlouse" aggregates (C) with a corresponding cryo-TEM image (D). Concentrations: 0.2 g/L (B), 0.1 g/L (C), and ~0.6 g/L (D). As no additional staining was performed, the contrast emerges solely from the iodide counterion of the P2VPq phase.

formation was gained from investigations of the intermediate structures obtained under comparable preparation conditions (Figure 2A). Here, the aggregates clearly consist of several intertwined and partially wrapped-up cylindrical micelles. Again, the dimensions of the cylinders are in good agreement with the diameter of the spherical micelles ($d_{cylinder}$ = 27.5 ± 2.5 nm, as compared to $d_{micelle}$ = 24.5 ± 2.0 nm), which corroborates the assumption that spherical micelles are indeed the underlying building blocks. Staining with OsO_4 reveals a PB (or mixed PB/P*t*BMA) core of the cylinders (Figure 2B). Subsequently, these cylinders align in a parallel, ribbon-like fashion, which we regard as another intermediate level on the way toward highly periodic lamellar "woodlice". Our assumption of a mixed PB/P*t*BMA core is further supported by the calculated phase segregation parameter, for PB/P*t*BMA, $\chi N \sim 1.1$.[48] According to the theory of phase separation for diblock copolymers, this is in the disordered regime due to the small degrees of polymerization for our system.[49,50] Furthermore, cast films of PB-*b*-P*t*BMA diblock copolymers with comparable molecular weights did not show any phase separation in the bulk (results not shown).

Cryo-TEM shows highly intertwined and entangled cylindrical micelles (Figure 2C). A surprisingly highly regular packing of individual cylinders can be observed in some cases, highlighted in the insets and gray scale analysis of Figure 2C. Remarkably, some of the structures show long-range order and dimensions of up to 1 μm in length.

With the example of these intermediate structures, we further investigated the influence of two other parameters during the process of structure formation (for details see Supporting Information): (i) the solutions were thermally annealed, and (ii) the time between quaternization in dioxane and dialysis to water was increased to up to 1 month. Whereas thermal annealing did not result in higher structural perfection at all, the structures were slightly more developed after 1 month in dioxane prior to dialysis (Figure S5). Nonetheless, from all of the TEM investigations discussed so far, different levels of hierarchy from approximately 20 nm to 1 μm were detected for μ-BVqT, starting from spherical micelles (level 1), which aggregate into cylinders (level 2), and finally into multilamellar superstructures (level 3).

Importance of the Nature of the Counterion. It is known that methyl iodide can undergo photodecomposition to form free iodine.[51] Based on this fact, one hypothesis for the observed structural differences was the presence of varying amounts of elementary iodine in the

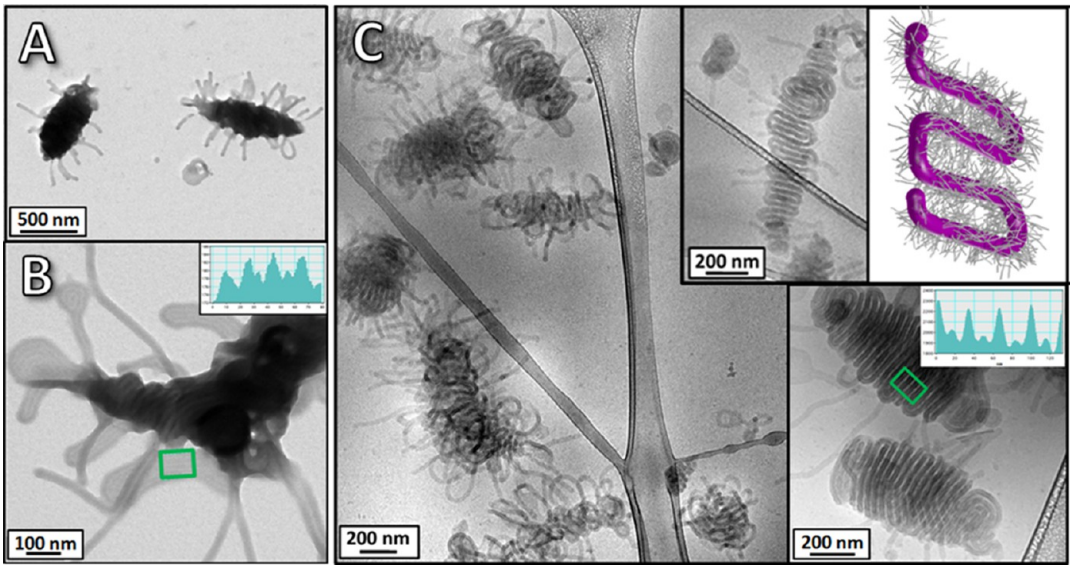

Figure 2. TEM (A,B) and cryo-TEM micrographs (C) of intermediate micellar structures from μ-BVqT in aqueous solution. The final polymer concentration was 0.2 g/L for TEM and 0.4 g/L for cryo-TEM. Whereas for (A) no staining was performed, the sample in (B) was stained with OsO_4. Here, the gray scale analysis of the highlighted area reveals a ribbon-like arrangement of cylinders.

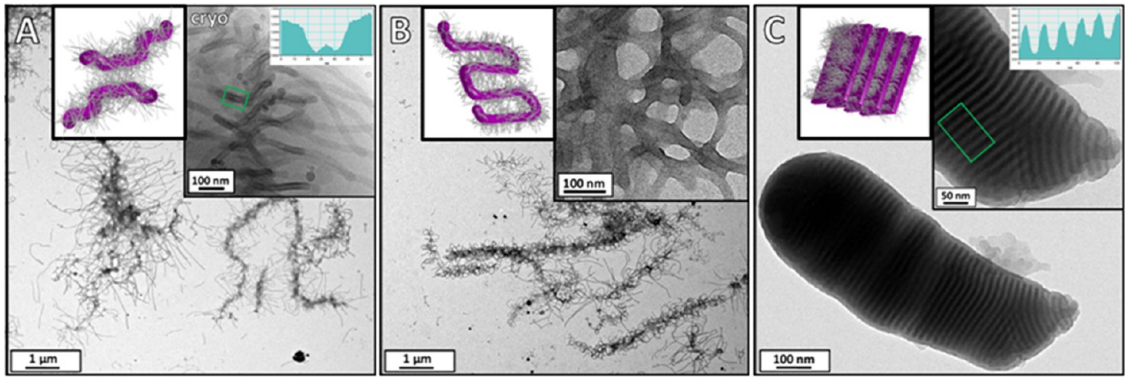

Figure 3. TEM micrographs from 0.2 g/L aqueous micellar solutions of μ-BVqT after dialysis in the presence of different amounts of iodine. The solutions were prepared with 0.08 (A), 0.25 (B), and 0.42 (C) equiv of iodine with respect to P2VPq monomer units. The inset in (A) shows the corresponding cryo-TEM micrograph. The schematic illustrations represent the dominant aggregate morphology. For the respective sample without additional iodine, see Figure 1B.

respective dioxane solutions. In combination with the iodide counterion, this then forms triiodide, I_3^-, which is a strongly polarizable counterion,[52,53] already described for quaternized poly(4-vinylpyridine) (P4VPq).[54] The increased hydrophobicity of P2VPq with triiodide as counterion is clearly demonstrated by DLS measurements of a P2VPq homopolymer in water (Figure S8). Higher amounts of added iodine led to an increase of the hydrodynamic radii, which we assign to hydrophobic interactions. In contrast, chloride or methyl sulfate counterions did not lead to the formation of any hierarchically structured aggregates for the μ-BVqT system (see Supporting Information).

However, addition of supplementary iodine to an aqueous micellar solution of μ-BVqT (Figure 1B) did not induce significant structural changes. We attribute this to two different reasons: first, owing to the reduced core dynamics, rearrangement processes are suppressed. Second and most important, iodine itself is not soluble in water but is solubilized by the formation of triiodide. However, the iodide counterions are mainly located within the micellar corona—approximately 90% according to investigations of quaternized poly(*N*,*N*-dimethylaminoethyl methacrylate) stars[55]—leading to very slow exchange processes. Consequently, we added different amounts of iodine to the μ-BVqT solution in dioxane prior to dialysis. The samples were allowed to equilibrate for 2 h to guarantee the conversion to triiodide and then dialyzed to water. Already the addition of 0.08 equiv of I_2 induced drastic structural changes (Figure 3A), as worm-like micelles and elongated superstructures were observed in contrast to spherical micelles in the absence of iodine (Figure 1B). Again, the diameter of these cylindrical aggregates refers to the initially observed spherical micelles ($d_{micelle} = 24.5 \pm 2.0$ nm and $d_{cylinder} = 25.0 \pm 2.0$ nm). The corona-forming

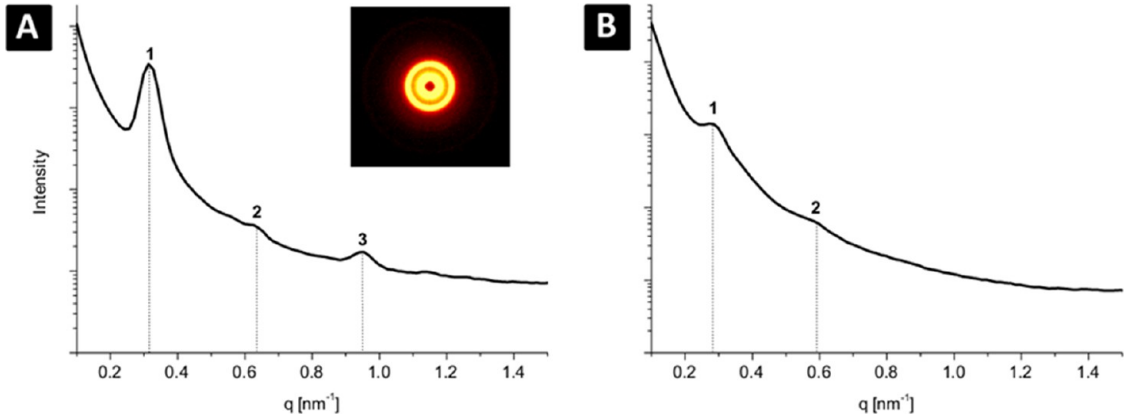

Figure 4. SAXS pattern of a freeze-dried powder from (A) the "woodlouse" structure (Figure 3C) and (B) the intermediate structure (Figure S5). The integer numbers indicate the relative reflex positions, and the inset in A depicts the scattering pattern observed at the 2D detector.

P2VPq block can be clearly distinguished in cryo-TEM (inset in Figure 3A and Figure S9A). For 0.25 equiv, almost exclusively superstructures from aggregated and intertwined cylindrical micelles are found. In addition, fewer protrusions and an increased tendency of the cylinders to form meander-like structures were observed. The inset in Figure 3B depicts an area where the cylinders form prestages of ribbons. When 0.42 equiv of I_2 was added, "woodlouse" aggregates with a periodic, multilayered structure were found (d_{lam} = 19.5 ± 1.0 nm, Figure 3C). This pattern is also clearly visible in cryo-TEM, accompanied by areas where the lamellae are less densely packed (highlighted area in Figure S9B) or particles which seem to be trapped as cylindrical superstructures (inset in Figure S9B). A minor fraction of micelles and cylinders was found, as well.

To evaluate this lamellar packing within the particles in more detail, additional SAXS measurements were conducted from freeze-dried powders of the sample depicted in Figure 3C. The SAXS pattern (Figure 4A) shows peaks with a q ratio of 1:2:3, representing the [100], [200], and [300] reflections, thus confirming the lamellar structure. The long period was calculated to d_{lam} = 20.0 ± 1.5 nm and is in perfect agreement with the values observed in TEM (d_{lam} = 19.5 ± 1.0 nm). In the SAXS pattern for the intermediate structure (as shown in Figure S5), the reflections were less pronounced (Figure 4B). This was already expected from the TEM images (Figure S5), which reveal a less regular arrangement. However, the assumption of an overall lamellar morphology and the presence of the [100] and [200] reflections allow the calculation of d_{lam} = 22.5 ± 2.0 nm. Comparable long periods from "woodlice" and aggregated cylinders further support our proposed mechanism of superstructure formation.

These different levels of hierarchical self-assembly of μ-BVqT into spherical micelles (level 1), followed by cylinders (level 2), superstructures thereof and, finally, the stacking and back-folding of lamellae into compartmentalized micrometer-sized polymer particles (level 3) can be attributed to surface minimization due to decreasing hydrophilicity of the P2VPq corona triggered by the presence of triiodide counterions. Hereby, the superstructure formation of lamellae *via* folding (or stacking) is supported by simulations on the sphere-cylinder-lamella transition in diblock copolymer systems.[56] As we are most probably dealing with non-equilibrium structures formed during dialysis, the folded cylinders are supposed to be transient intermediate structures on the way toward lamellae. Similar structures were already reported for linear ABC triblock terpolymers, where either the addition of a diamine in the case of poly(acrylic acid) as solubilizing block[31−33] or changes in solvent quality for the P2VP corona[23] triggered the formation of superstructures. However, in our case, this is clearly caused by changes in the polarizability of the counterion, triggered by the addition of iodine. The amount of triiodide represents the essential trigger here. Both the assembly pathway and a delicate balance of iodide/triiodide regulate structural precision and the overall colloidal stability of the substructured particles. Furthermore, here, the well-defined compact structures clearly evolve through a complex aggregation and fusion *via* cylindrical building units in contrast to the stacking of disk-like structures as reported in literature.[23,31−33] The system presented here is relatively simple as no sophisticated preparation pathways utilizing bifunctional additives have to be applied, and the structures are obtained in aqueous solution rather than in solvent mixtures. Also, the directed self-assembly is induced by the monovalent counterion, and the structural integrity is rather unaffected by the pH of the solution (see aggregates within acidic media of pH 3 as depicted in Figure S10).

Structural Characterization of "Woodlouse" Aggregates. So far, we have described the triiodide-mediated hierarchical self-assembly of μ-BVqT into compartmentalized particles. The highly periodic internal fine structure is confirmed by gray scale analysis of the TEM micrographs

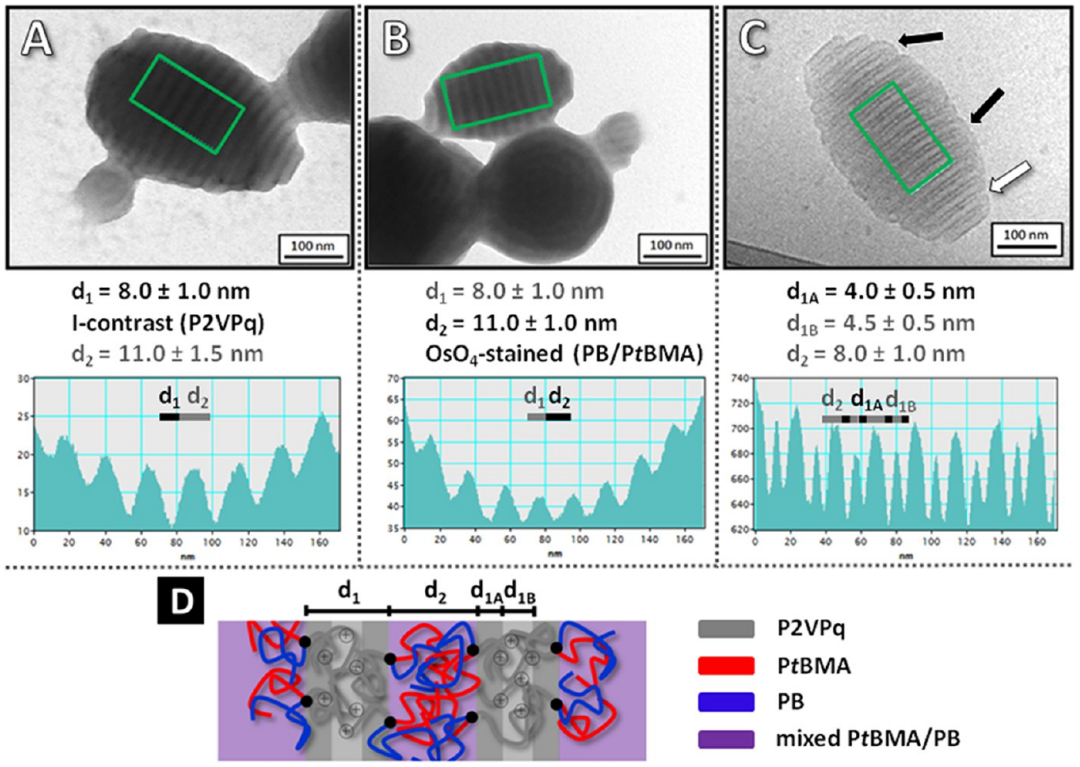

Figure 5. TEM micrographs of "woodlouse" aggregates of μ-BVqT obtained *via* dialysis from dioxane into water (A,B). The concentration was 0.1 g/L. In (A), the contrast emerges solely from the iodide counterion of the P2VPq phase, whereas (B) was stained with OsO_4. In cryo-TEM (C), a regular pattern of three distances is visible. The concentration was 0.6 g/L. The corresponding gray scale analyses are shown below the micrographs. The proposed arrangement of the miktoarm star terpolymers is illustrated in (D).

of individual particles (Figure 5A). Here, the darker domains correspond to the P2VPq phase containing iodide/triiodide counterions (d_1 = 8 nm), whereas the contrast is inverted when staining with OsO_4 was performed (selective for the PB phase, d_2 = 11 nm Figure 5B). The wider lamellae presumably consist of a mixed P*t*BMA/PB phase as already discussed above.

In cryo-TEM, even three different repeating distances are visible (Figure 5C). Here, the observed periodicities can be explained in a similar way. The 8 nm of d_2 represent a mixed phase of PB and P*t*BMA, which is slightly broadened in TEM (d_2 in Figure 5B), as the lamella is flattened and collapsed onto the carbon film in the dried state. On the other hand, both d_{1A} and d_{1B} represent P2VPq, serving as the corona for the mixed PB/P*t*BMA domains. At the interface (d_{1A}), the density of P2VPq chains is higher as compared to the periphery (d_{1B}), leading to an increased electron density. The proposed chain packing and the corresponding dimensions are illustrated in Figure 5D. Hereby, the individual lamellar sheets of the superstructures can either stack (white arrow in Figure 5C) or back-fold (black arrows in Figure 5C), leading to "open" or "closed" structures at the edge of the particles.

We additionally performed cryo-TEM at different tilt angles (Figure S11 and video S3). Thereby, the influence of the "woodlouse" orientation within the vitrified film was examined, and from the projections at different tilt angles, a circular cross section of the aggregates can be clearly deduced. Again, the presence of flat two-dimensional assemblies can be excluded, which is additionally supported by SEM of the dried particles (Figure S12). In the cryo-TEM tilt images, the internal fine structure is only visible if the particles are oriented perpendicular to the beam direction. If the stage is tilted further, the structural features blur and, finally, disappear completely. The fact that such structural features are only visible under specific viewing angles has already been observed.[57]

Cross-sectional analysis of the "woodlice" within thin film cuts of epoxy resin embedded particles (Figure 6A and Figure S13) clearly showed a periodic fine structure, further confirming our assumption that the particles are not hollow. When the sample was treated with OsO_4 (staining of PB, Figure 6A), undulated lamellae are visualized as already discussed for the intermediate structures. The rather undulated shape of the PB/P*t*BMA lamella might be related to partial demixing of PB and P*t*BMA, despite the rather low χN. This could be a consequence of the longer DP of the PB block (109) as compared to P*t*BMA (DP = 53), as well as different χ for the PB/P2VP and the P*t*BMA/P2VP interactions, leading to minimization of the PB/P2VP interface.[48,58] Additionally, from DSC measurements of the miktoarm

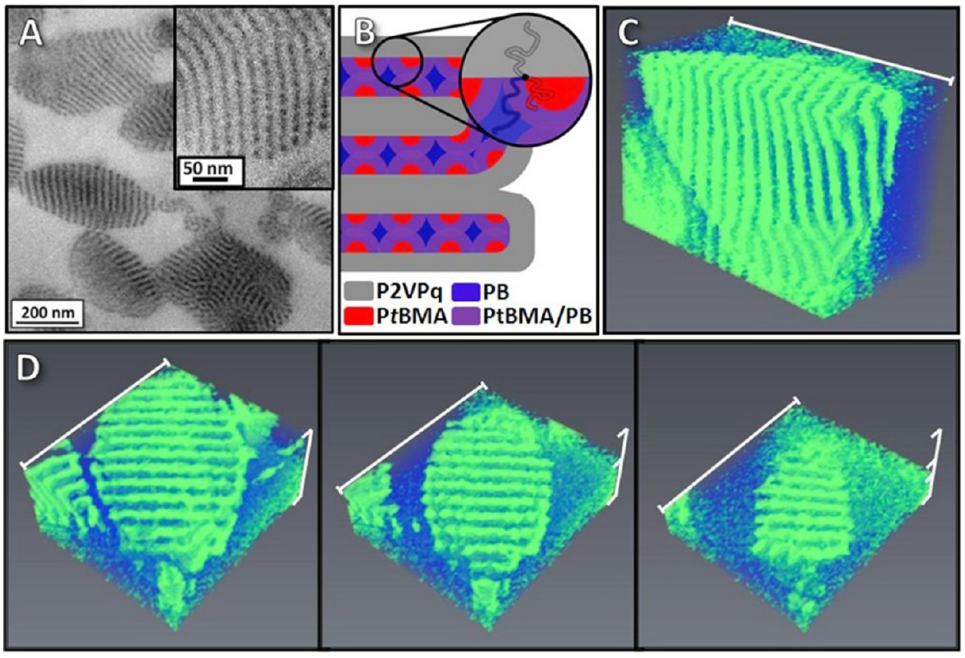

Figure 6. (A) TEM micrograph of 50 nm thick cuts from freeze-dried and embedded samples of μ-BVqT aggregates, stained with OsO_4. (B) Schematic illustration of the block arrangement within the "woodlouse" structure is depicted, with the two possibilities of bent (upper part) and stacked lamellae (lower part). The gray areas resemble the P2VPq phase; P*t*BMA is red, and PB is blue. The violet domains represent a mixed PB/P*t*BMA phase. TEM tomography 3D reconstructions of a slice of the "woodlouse" structure (C) and cross-sectional analysis of a single particle (D). The tomography images were obtained from a 150 nm thick cut, which was additionally treated with OsO_4 to selectively stain the mixed PB/P*t*BMA phase (plotted in green). The approximate length of the long marked edge of the reconstructions is 280 nm in (C) and 220 nm in (D).

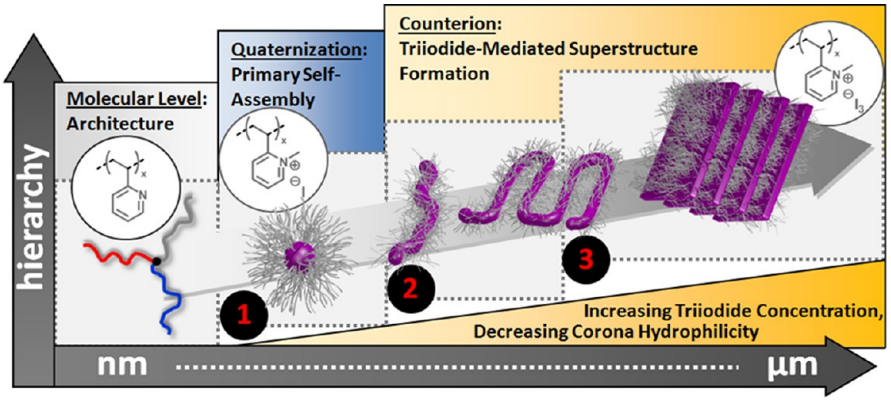

Figure 7. Proposed mechanism for the triiodide-triggered superstructure formation of the μ-BVqT miktoarm star terpolymer *via* different hierarchy levels from the nanometer to the micrometer scale: spherical micelles (level 1), cylindrical micelles (level 2), and lamellar superstructures (level 3).

star terpolymer, the presence of a T_g at -2 °C also hints toward the presence of a separated PB phase in the bulk state (Figure S14). This leads to a direct P*t*BMA/P2VPq interface, accompanied by an interface of P2VPq with the adjacent mixed PB/P*t*BMA phase and, finally, a pure PB domain without a PB/P2VPq interface. The proposed arrangement of the constituting segments is illustrated in Figure 6B. Staining with OsO_4 enhances contrast mainly in the PB phase, but also the mixed phase appears darker (Figure 6A), whereas the pure P*t*BMA domains appear brighter. Similarly, the TEM micrographs of the cylindrical intermediate aggregates under the same sample preparation method also hint toward an undulated phase boundary (Figure S6B).

Finally, the volume morphology of the "woodlice" was investigated using TEM tomography (TEMT). We therefore prepared thicker slices (~150 nm) of the resin-embedded sample and performed staining with OsO_4 to provide maximum contrast. In Figure 6C, a three-dimensional reconstruction of a slice of a woodlouse particle with view into the lamellar bulk morphology is shown. Additionally, Figure 6D shows three different slices of the same reconstruction for a single particle. Both three-dimensional reconstructions clearly confirm the presence of lamellae with an undulated

surface throughout the entire sample (also see video S4). Hereby, the formation of well-defined lamellar structures as compared to micellar clusters (observed for linear polymers; see Figure S4) is probably a direct consequence of the miktoarm architecture. In accordance with both theory and experimental work,[59] the increased segmental density has a distinctive effect on the surface curvature and, in the case of our system, facilitates the formation of lamellae with low surface curvature.

CONCLUSIONS

We have demonstrated the hierarchical self-assembly of an ABC miktoarm star terpolymer into substructured particles of up to 1 μm in size, which we term "woodlouse" particles. Spherical micelles with a mixed PB/P*t*BMA core and a P2VPq corona act as the basic building blocks (level 1). Stepwise aggregation of these results in cylindrical micelles (level 2), followed by superstructures thereof, and finally compartmentalized particles of up to 1 μm in size. These particles feature a highly periodic, lamellar fine structure (level 3). The presence and amount of triiodide as a highly polarizable counterion for the P2VPq corona is an essential trigger to induce this superstructure formation into different levels of hierarchy (Figure 7). All intermediates of increasing hierarchy involved on the way to the final "woodlice" are visualized by TEM and cryo-TEM. The iodide/triiodide system is an elegant approach for directing the hierarchical self-assembly of such materials. The nature of the counterion, the miktoarm star architecture, and the assembly pathway are essential parameters and influence structural perfection and the final morphology. To recapitulate, a detailed understanding of the self-assembly mechanism into complex superstructures was obtained, which bear structural similarities to biological systems such as mitochondria. Applying these results to other miktoarm star terpolymer systems with higher segmental incompatibility might lead to completely phase-separated cores and represents an interesting approach to core-compartmentalized structures of complex shape. Further functionalization and modification of these structures will enable the preparation of a variety of stimuli-responsive highly structured materials with defined internal periodicity.

The question arises whether this approach is applicable to other miktoarm star systems containing polycationic segments in general or whether the combination of P2VPq and a "dynamic", low T_g segment like PB is a prerequisite. This will be the subject of future work. The use of iodide/triiodide as a set screw to direct the self-assembly of different materials into well-defined hierarchical superstructures would be advantageous and desirable.

EXPERIMENTAL SECTION

Materials. Butadiene (Riessner-Gase) was passed through columns filled with molecular sieves (4 Å) and basic aluminum oxide and stored over dibutylmagnesium (1 M solution in heptane, Aldrich). 2-Vinylpyridine (Aldrich) was degassed, stirred with triethylaluminum (1 M solution in hexanes, Aldrich), and condensed on a high vacuum line. THF (Sigma-Aldrich) was distilled from CaH_2 and Na/K alloy. *sec*-Butyllithium (Acros, 1.3 M in cyclohexane/hexane: 92/8) was used without further purification. *tert*-Butyl methacrylate (*t*BMA, Sigma-Aldrich) for ATRP was filtered over basic aluminum oxide. *N*,*N*,*N*′,*N*′,*N*″-Pentamethyldiethylenetriamine (PMDETA) and CuBr were purchased from Aldrich and distilled and degassed or treated with pure acetic acid and filtered, respectively. 1-[(4-(*tert*-Butyldimethylsilyl)-ethynyl)phenyl]-1-phenylethylene was synthesized from 1-(4-bromophenyl)-1-phenylethylene as already reported.[36] The aqueous solutions were prepared with distilled desalinated water. All other chemicals were of analytical grade and used as received. The dialysis membrane used for all steps was purchased from Roth (Spectra Por), with a molecular weight cutoff (MWCO) of 1000 g/mol.

Synthesis of Polybutadiene-*arm*-Poly(2-vinylpyridine)-*arm*-Poly(*tert*-butyl methacrylate) (μ-BVT) Miktoarm Star Terpolymer. The detailed procedures for the synthesis of the individual polymeric building blocks and the ligation by azide–alkyne Huisgen cycloaddition have already been reported elsewhere.[36] The alkyne mid-functionalized diblock copolymer polybutadiene-*b*-poly(2-vinylpyridine) (PB-*b*-P2VP) was synthesized *via* anionic polymerization using an alkyne-substituted DPE. The poly(*tert*-butyl methacrylate) (P*t*BMA) arm was synthesized in a separate polymerization procedure *via* ATRP using an azido-functionalized initiator.[60]

Finally, the ligation of the alkyne-functionalized diblock copolymer with the azido-functionalized homopolymer was conducted by azide–alkyne Huisgen cycloaddition.[61] Therefore, a mixture of the diblock copolymer and 1.1 equiv of the homopolymer was dissolved in THF at a concentration of ~20 g/L and degassed for 10 min. After addition of 1 equiv of CuBr, the solution was degassed for further 15 min. PMDETA (1 equiv) was added to complex the copper and start the reaction, which was followed by SEC. After 2 days, the resulting miktoarm star terpolymer was purified by passing the solution through a small column with basic alumina to remove copper and finally freeze-dried from dioxane.

Quaternization of μ-BVT and Preparation of Aqueous Micellar Solutions. The transformation of the P2VP compartment into a strong cationic polyelectrolyte (P2VPq) was conducted using methyl iodide as quaternization agent. The miktoarm star terpolymer was dissolved in dioxane at a concentration of 2 g/L. After the addition of a 10-fold excess of methyl iodide compared to 2VP units, the solution was allowed to stir at room temperature for 3 days. To remove excess quaternization agent, the solution was dialyzed against dioxane. During this step, the solution typically turned yellow. Finally, the solution was diluted with dioxane to obtain a concentration of 1 g/L, and then the solvent was subsequently exchanged against water. The dialysis water was changed three times. The concentrations of the obtained aqueous solutions ranged from 0.3 to 0.7 g/L. It was observed that some samples precipitated after a few days or weeks, whereas others were still colloidally stable after 2 years (even though prepared under comparable conditions). As the amount of triiodide was proven to be responsible for the different aggregation structure, we attribute subtle differences in the ratio of iodide/triiodide to have an impact on the long-term stability of the "woodlouse" aggregates.

To simplify matters, in the case of all quaternized solutions, the given concentrations resemble the concentration of the pristine miktoarm star terpolymer before quaternization, thus neglecting the increase of mass due to quaternization.

For the preparation of the triiodide complexes, an iodine stock solution was prepared with dioxane as solvent at 15 g/L. Then, this iodine solution was added to the agitated dioxane solution of the quaternized star terpolymer until the desired ratio of iodine to 2VP was achieved. Afterward, the solutions were stirred for 2 h and then treated with ultrasound for 15 min. Subsequently, the solutions were dialyzed against water, as described above. The solutions were obtained with concentrations ranging from 0.3 to 0.7 g/L. Whereas the solutions with low iodine contents were long-term stable, the solutions with high amounts of iodine slowly precipitated with time. However, these solutions were easily redispersible by shaking without leaving macroscopic precipitate.

Transmission Electron Microscopy (Cryo-TEM and TEM). TEM micrographs were taken with a Zeiss CEM 902 or 922 OMEGA electron microscope operated at 80 or 200 kV, respectively. Both machines were equipped with an in-column energy filter. For sample preparation, 2 μL of the solution (typically 0.1−0.2 g/L) was deposited on a TEM grid (copper, 200 mesh). Afterward, the remaining solvent was removed with a blotting paper. For investigation of the particle films, the freeze-dried polymer was embedded into a resin (EpoTek 301). Then, 50 nm thin cuts were prepared with a Leica EM UC7 microtome equipped with a diamond knife and deposited onto TEM grids (copper, 200 mesh). Selective staining of the B phase was achieved by treating the samples with OsO_4 vapor for 30 s.

For cryo-TEM studies, a drop (~2 mL) of the aqueous micellar solution ($c \approx 0.4-0.7$ g/L) was placed on a lacey carbon-coated copper TEM grid (200 mesh, Science Services), where most of the liquid was removed with blotting paper, leaving a thin film stretched over the grid holes. The specimens were shock vitrified by rapid immersion into liquid ethane in a temperature-controlled freezing unit (Zeiss Cryobox, Zeiss NTS GmbH) and cooled to approximately 90 K. The temperature was monitored and kept constant in the chamber during all of the preparation steps. After freezing the specimens, they were inserted into a cryo-transfer holder (CT3500, Gatan) and transferred to a Zeiss EM922 OMEGA EFTEM instrument. Examinations were carried out at temperatures around 90 K. The microscope was operated at an acceleration voltage of 200 kV. Zero-loss filtered images (DE $^1/_4$ 0 eV) were taken under reduced dose conditions. All images were registered digitally by a bottom-mounted CCD camera system (Ultrascan 1000, Gatan), combined, and processed with a digital imaging processing system (Gatan Digital Micrograph 3.9 for GMS 1.4).

Evaluation of the respective length scales of the structures was achieved by measuring 50−100 different spots within the sample with the UTHSCSA ImageTool V. 3.00.

TEM Tomography (TEMT). For TEMT measurements, samples (~200 nm thickness) were microtome cut onto Cu mesh grids with a carbon film and an additional underlying polyvinyl formal coating. Prior to TEMT, samples were stained using OsO_4 vapor and Au nanoparticles with a diameter of approximately 5 nm (BB International Ltd., UK) were deposited onto the miktoarm star terpolymer films. TEMT measurements were performed on a JEM-2200FS (JEOL Co., Ltd., Japan) at an accelerating voltage of 200 kV and equipped with a slow-scan CCD camera (GATAN USC4000, Gatan Inc., USA). The TEM micrographs were obtained at 1° increment between −65° and 65° tilt angle. The image set was processed according to the same protocol described elsewhere.[62] Subsequently, the tilt series of the TEM images were aligned by using the previously deposited Au nanoparticles as fiducial markers and then reconstructed on the basis of the filtered back-projection (FBP) method.[63] The reconstructed images were further visualized using the software platform Avizo (Visualization Sciences Group, http://www.vsg3d.com).

Small-Angle X-ray Scattering (SAXS). SAXS measurements of the freeze-dried powders were performed on a Bruker AXS Nanostar (Bruker, Karlsruhe, Germany), equipped with a microfocus X-ray source (Incoatec IμS$_{Cu}$ E025, Incoatec Geesthacht, Germany), operating at λ = 1.54 Å. A pinhole setup with 750, 400, and 1000 μm (in the order from source to sample) was used, and the sample-to-detector distance was 107 cm. Samples were mounted on a metal rack and fixed using tape. The scattering patterns were corrected for the beam stop and the background (Scotch tape) prior to evaluations. The measurement time for the samples was 4 h in all cases.

Conflict of Interest: The authors declare no competing financial interest.

Acknowledgment. This work was supported by the Deutsche Forschungsgesellschaft within SPP 1165 (Mu896/22). We thank Prof. M. Ballauff, D.V. Pergushov, and H. Schmalz for fruitful discussions. F. Wieberger is acknowledged for performing some of the SEM measurements, and A. Pfaffenberger for recording some of the TEM micrographs. H.J. gratefully acknowledges the financial support received through Grants-in-Aid No. 24310092 from the Ministry of Education, Culture, Sports, Science, and Technology. F.H.S. acknowledges a fellowship from the Verband der Chemischen Industrie (VCI) and funding from the Thuringian Ministry for Education, Science and Culture (TMBWK, Grant No. B514-09051, NanoConSens, and Grant No. B515-11028, SWAXS-JCSM).

Supporting Information Available: Additional experimental section. Molecular characterization and SEC eluograms of μ-BVT and its precursor polymers. DLS of micellar μ-BVqT solution and P2VPq homopolymer. DSC of μ-BVT. Additional SEM, TEM, and cryo-TEM of micellar aggregates. Videos of cryo-TEM tilt series and a TEM tomography 3D reconstruction. This material is available free of charge *via* the Internet at http://pubs.acs.org.

Note Added after ASAP Publication. This manuscript was published on the Web on April 9, 2013. The TOC/Abstract graphic was replaced and the revised version was reposted on April 12, 2013.

REFERENCES AND NOTES

1. Whitesides, G. M.; Grzybowski, B. Self-Assembly at All Scales. *Science* **2002**, *295*, 2418–2421.
2. Zhang, S. Emerging Biological Materials through Molecular Self-Assembly. *Biotechnol. Adv.* **2002**, *20*, 321–339.
3. Nagarajan, R.; Ruckenstein, E. Theory of Surfactant Self-Assembly: A Predictive Molecular Thermodynamic Approach. *Langmuir* **1991**, *7*, 2934–2969.
4. Svenson, S. Controlling Surfactant Self-Assembly. *Curr. Opin. Colloid Interface Sci.* **2004**, *9*, 201–212.
5. Zhang, L.; Eisenberg, A. Multiple Morphologies of "Crew-Cut" Aggregates of Polystyrene-*b*-Poly(acrylic acid) Block Copolymers. *Science* **1995**, *268*, 1728–1731.
6. Mai, Y.; Eisenberg, A. Self-Assembly of Block Copolymers. *Chem. Soc. Rev.* **2012**, *41*, 5969–5985.
7. Antonietti, M.; Förster, S. Vesicles and Liposomes: A Self-Assembly Principle beyond Lipids. *Adv. Mater.* **2003**, *15*, 1323–1333.
8. Hamley, I. W. Nanotechnology with Soft Materials. *Angew. Chem., Int. Ed.* **2003**, *42*, 1692–1712.
9. Schacher, F. H.; Rupar, P. A.; Manners, I. Functional Block Copolymers: Nanostructured Materials with Emerging Applications. *Angew. Chem., Int. Ed.* **2012**, *51*, 7898–7921.
10. Savić, R.; Luo, L.; Eisenberg, A.; Maysinger, D. Micellar Nanocontainers Distribute to Defined Cytoplasmic Organelles. *Science* **2003**, *300*, 615–618.
11. Cabral, H.; Matsumoto, Y.; Mizuno, K.; Chen, Q.; Murakami, M.; Kimura, M.; Terada, Y.; Kano, M. R.; Miyazono, K.; Uesaka, M.; *et al.* Accumulation of Sub-100 nm Polymeric Micelles in Poorly Permeable Tumours Depends on Size. *Nat. Nanotechnol.* **2011**, *6*, 815–823.
12. Holder, S. J.; Sommerdijk, N. A. J. M. New Micellar Morphologies from Amphiphilic Block Copolymers: Disks, Toroids and Bicontinuous Micelles. *Polym. Chem.* **2011**, *2*, 1018–1028.
13. Bates, F. S.; Hillmyer, M. A.; Lodge, T. P.; Bates, C. M.; Delaney, K. T.; Fredrickson, G. H. Multiblock Polymers: Panacea or Pandora's Box? *Science* **2012**, *336*, 434–440.
14. Li, Z.; Kesselman, E.; Talmon, Y.; Hillmyer, M. A.; Lodge, T. P. Multicompartment Micelles from ABC Miktoarm Stars in Water. *Science* **2004**, *306*, 98–101.
15. Li, Z.; Hillmyer, M. A.; Lodge, T. P. Morphologies of Multicompartment Micelles Formed by ABC Miktoarm Star Terpolymers. *Langmuir* **2006**, *22*, 9409–9417.

16. Saito, N.; Liu, C.; Lodge, T. P.; Hillmyer, M. A. Multicompartment Micelles from Polyester-Containing ABC Miktoarm Star Terpolymers. *Macromolecules* **2008**, *41*, 8815–8822.
17. Liu, C.; Hillmyer, M. A.; Lodge, T. P. Multicompartment Micelles from pH-Responsive Miktoarm Star Block Terpolymers. *Langmuir* **2009**, *25*, 13718–13725.
18. Kubowicz, S.; Baussard, J.-F.; Lutz, J.-F.; Thünemann, A. F.; von Berlepsch, H.; Laschewsky, A. Multicompartment Micelles Formed by Self-Assembly of Linear ABC Triblock Copolymers in Aqueous Medium. *Angew. Chem., Int. Ed.* **2005**, *44*, 5262–5265.
19. Fang, B.; Walther, A.; Wolf, A.; Xu, Y.; Yuan, J.; Müller, A. H. E. Undulated Multicompartment Cylinders by the Controlled and Directed Stacking of Polymer Micelles with a Compartmentalized Corona. *Angew. Chem., Int. Ed.* **2009**, *48*, 2877–2880.
20. Schacher, F.; Betthausen, E.; Walther, A.; Schmalz, H.; Pergushov, D. V.; Müller, A. H. E. Interpolyelectrolyte Complexes of Dynamic Multicompartment Micelles. *ACS Nano* **2009**, *3*, 2095–2102.
21. Schacher, F.; Walther, A.; Müller, A. H. E. Dynamic Multicompartment-Core Micelles in Aqueous Media. *Langmuir* **2009**, *25*, 10962–10969.
22. Dupont, J.; Liu, G.; Niihara, K.-i.; Kimoto, R.; Jinnai, H. Self-Assembled ABC Triblock Copolymer Double and Triple Helices. *Angew. Chem., Int. Ed.* **2009**, *48*, 6144–6147.
23. Zhu, J.; Jiang, W. Self-Assembly of ABC Triblock Copolymer into Giant Segmented Wormlike Micelles in Dilute Solution. *Macromolecules* **2005**, *38*, 9315–9323.
24. Gröschel, A. H.; Schacher, F. H.; Schmalz, H.; Borisov, O. V.; Zhulina, E. B.; Walther, A.; Müller, A. H. E. Precise Hierarchical Self-Assembly of Multicompartment Micelles. *Nat. Commun.* **2012**, *3*, 710.
25. Gröschel, A. H.; Walther, A.; Löbling, T. I.; Schmelz, J.; Hanisch, A.; Schmalz, H.; Müller, A. H. E. Facile, Solution-Based Synthesis of Soft, Nanoscale Janus Particles with Tunable Janus Balance. *J. Am. Chem. Soc.* **2012**, *134*, 13850–13860.
26. Wang, H.; Lin, W.; Fritz, K. P.; Scholes, G. D.; Winnik, M. A.; Manners, I. Cylindrical Block Co-micelles with Spatially Selective Functionalization by Nanoparticles. *J. Am. Chem. Soc.* **2007**, *129*, 12924–12925.
27. Wang, X.; Guerin, G.; Wang, H.; Wang, Y.; Manners, I.; Winnik, M. A. Cylindrical Block Copolymer Micelles and Co-micelles of Controlled Length and Architecture. *Science* **2007**, *317*, 644–647.
28. Rupar, P. A.; Chabanne, L.; Winnik, M. A.; Manners, I. Non-centrosymmetric Cylindrical Micelles by Unidirectional Growth. *Science* **2012**, *337*, 559–562.
29. Schmelz, J.; Karg, M.; Hellweg, T.; Schmalz, H. General Pathway toward Crystalline-Core Micelles with Tunable Morphology and Corona Segregation. *ACS Nano* **2011**, *5*, 9523–9534.
30. Cui, H.; Chen, Z.; Zhong, S.; Wooley, K. L.; Pochan, D. J. Block Copolymer Assembly *via* Kinetic Control. *Science* **2007**, *317*, 647–650.
31. Cui, H.; Chen, Z.; Wooley, K. L.; Pochan, D. J. Controlling Micellar Structure of Amphiphilic Charged Triblock Copolymers in Dilute Solution *via* Coassembly with Organic Counterions of Different Spacer Lengths. *Macromolecules* **2006**, *39*, 6599–6607.
32. Li, Z.; Chen, Z.; Cui, H.; Hales, K.; Wooley, K. L.; Pochan, D. J. Controlled Stacking of Charged Block Copolymer Micelles. *Langmuir* **2007**, *23*, 4689–4694.
33. Pochan, D. J.; Chen, Z.; Cui, H.; Hales, K.; Qi, K.; Wooley, K. L. Toroidal Triblock Copolymer Assemblies. *Science* **2004**, *306*, 94–97.
34. Cui, H.; Chen, Z.; Wooley, K. L.; Pochan, D. J. Origins of Toroidal Micelle Formation through Charged Triblock Copolymer Self-Assembly. *Soft Matter* **2009**, *5*, 1269–1278.
35. Chen, Z.; Cui, H.; Hales, K.; Li, Z.; Qi, K.; Pochan, D. J.; Wooley, K. L. Unique Toroidal Morphology from Composition and Sequence Control of Triblock Copolymers. *J. Am. Chem. Soc.* **2005**, *127*, 8592–8593.
36. Hanisch, A.; Schmalz, H.; Müller, A. H. E. A Modular Route for the Synthesis of ABC Miktoarm Star Terpolymers *via* a New Alkyne-Substituted Diphenylethylene Derivative. *Macromolecules* **2012**, *45*, 8300–8309.
37. Justynska, J.; Hordyjewicz, Z.; Schlaad, H. Toward a Toolbox of Functional Block Copolymers *via* Free-Radical Addition of Mercaptans. *Polymer* **2005**, *46*, 12057–12064.
38. Walther, A.; Göldel, A.; Müller, A. H. E. Controlled Cross-linking of Polybutadiene Containing Block Terpolymer Bulk Structures: A Facile Way towards Complex and Functional Nanostructures. *Polymer* **2008**, *49*, 3217–3227.
39. Martin, T. J.; Procházka, K.; Munk, P.; Webber, S. E. pH-Dependent Micellization of Poly(2-vinylpyridine)-*block*-poly(ethylene oxide). *Macromolecules* **1996**, *29*, 6071–6073.
40. Burkhardt, M.; Martinez-Castro, N.; Tea, S.; Drechsler, M.; Babin, I.; Grishagin, I.; Schweins, R.; Pergushov, D. V.; Gradzielski, M.; Zezin, A. B.; *et al.* Polyisobutylene-*block*-Poly(methacrylic acid) Diblock Copolymers: Self-Assembly in Aqueous Media. *Langmuir* **2007**, *23*, 12864–12874.
41. Saito, N.; Liu, C.; Lodge, T. P.; Hillmyer, M. A. Multicompartment Micelle Morphology Evolution in Degradable Miktoarm Star Terpolymers. *ACS Nano* **2011**, *4*, 1907–1912.
42. He, T.; Li, B.; Ren, S. Glass Transition Temperature and Chain Flexibility of 1,2-Polybutadiene. *J. Appl. Polym. Sci.* **1986**, *31*, 873–884.
43. Barton, A. F. M. *CRC Handbook of Polymer–Liquid Interaction Parameters and Solubility Parameters*; CRC Press: Boca Raton, FL, 1990.
44. Brandrup, J.; Immergut, E. H.; Grulke, E. A. *Polymer Handbook*, 4th ed.; Wiley: New York, 1999.
45. Pispas, S.; Hadjichristidis, N.; Potemkin, I.; Khokhlov, A. Effect of Architecture on the Micellization Properties of Block Copolymers: A_2B Miktoarm Stars *vs* AB Diblocks. *Macromolecules* **2000**, *33*, 1741–1746.
46. Kong, W.; Li, B.; Jin, Q.; Ding, D.; Shi, A.-C. Helical Vesicles, Segmented Semivesicles, and Noncircular Bilayer Sheets from Solution-State Self-Assembly of ABC Miktoarm Star Terpolymers. *J. Am. Chem. Soc.* **2009**, *131*, 8503–8512.
47. Wang, L.; Xu, R.; Wang, Z.; He, X. Kinetics of Multicompartment Micelle Formation by Self-Assembly of ABC Miktoarm Star Terpolymer in Dilute Solution. *Soft Matter* **2012**, *8*, 11462–11470.
48. Schacher, F.; Yuan, J.; Schoberth, H. G.; Müller, A. H. E. Synthesis, Characterization, and Bulk Crosslinking of Polybutadiene-*block*-Poly(2-vinyl pyridine)-*block*-Poly(*tert*-butyl methacrylate) Block Terpolymers. *Polymer* **2010**, *51*, 2021–2032.
49. Leibler, L. Theory of Microphase Separation in Block Copolymers. *Macromolecules* **1980**, *13*, 1602–1617.
50. Bates, F. S.; Fredrickson, G. H. Block Copolymer Thermodynamics: Theory and Experiment. *Annu. Rev. Phys. Chem.* **1990**, *41*, 525–557.
51. West, W.; Schlessinger, L. The Mechanism of the Photodecomposition of Methyl and Ethyl Iodides. *J. Am. Chem. Soc.* **1938**, *60*, 961–966.
52. Palmer, D. A.; Ramette, R. W.; Mesmer, R. E. Triiodide Ion Formation Equilibrium and Activity Coefficients in Aqueous Solution. *J. Solution Chem.* **1984**, *13*, 673–683.
53. Zhang, F. S.; Lynden-Bell, R. M. Interactions of Triiodide Cluster Ion with Solvents. *Eur. Phys. J. D* **2005**, *34*, 129–132.
54. Chernov'yants, M.; Burykin, I.; Pisanov, R.; Shalu, O. Synthesis and Antimicrobial Activity of Poly(*N*-methyl-4-vinylpyridinium triiodide). *Pharm. Chem. J.* **2010**, *44*, 61–63.
55. Plamper, F. A.; Schmalz, A.; Penott-Chang, E.; Drechsler, M.; Jusufi, A.; Ballauff, M.; Müller, A. H. E. Synthesis and Characterization of Star-Shaped Poly(*N*,*N*-dimethylaminoethyl methacrylate) and Its Quaternized Ammonium Salts. *Macromolecules* **2007**, *40*, 5689–5697.
56. Zhulina, E. B.; Adam, M.; LaRue, I.; Sheiko, S. S.; Rubinstein, M. Diblock Copolymer Micelles in a Dilute Solution. *Macromolecules* **2005**, *38*, 5330–5351.
57. McKenzie, B. E.; Nudelman, F.; Bomans, P. H. H.; Holder, S. J.; Sommerdijk, N. A. J. M. Temperature-Responsive Nanospheres with Bicontinuous Internal Structures from a Semicrystalline Amphiphilic Block Copolymer. *J. Am. Chem. Soc.* **2010**, *132*, 10256–10259.

58. Schacher, F. H.; Sugimori, H.; Hong, S.; Jinnai, H.; Müller, A. H. E. Tetragonally Perforated Lamellae of Polybutadiene-*block*-Poly(2-vinylpyridine)-*block*-Poly(*tert*-butyl methacrylate) (BVT) Triblock Terpolymers in the Bulk: Preparation, Cross-Linking, and Dissolution. *Macromolecules* **2012**, *45*, 7956–7963.
59. Dyer, C.; Driva, P.; Sides, S. W.; Sumpter, B. G.; Mays, J. W.; Chen, J.; Kumar, R.; Goswami, M.; Dadmun, M. D. Effect of Macromolecular Architecture on the Morphology of Polystyrene-Polyisoprene Block Copolymers. *Macromolecules* **2013**, *46*, 2023–2031.
60. Mantovani, G.; Ladmiral, V.; Tao, L.; Haddleton, D. M. One-Pot Tandem Living Radical Polymerisation-Huisgens Cycloaddition Process ("Click") Catalysed by *N*-Alkyl-2-pyridylmethanimine/Cu(i)Br Complexes. *Chem. Commun.* **2005**, *0*, 2089–2091.
61. Binder, W. H.; Sachsenhofer, R. `Click' Chemistry in Polymer and Materials Science. *Macromol. Rapid Commun.* **2007**, *28*, 15–54.
62. Jinnai, H.; Spontak, R. J.; Nishi, T. Transmission Electron Microtomography and Polymer Nanostructures. *Macromolecules* **2010**, *43*, 1675–1688.
63. Crowther, R. A.; DeRosier, D. J.; Klug, A. The Reconstruction of a Three-Dimensional Structure from Projections and its Application to Electron Microscopy. *Proc. R. Soc. London A* **1970**, *317*, 319–340.